On the estimate of the stochastic layer width for a model of tracer dynamics

José L. Trueba and José P. Baltanás
Nonlinear Dynamics and Chaos Group, Departamento de Matemáticas y Física Aplicadas y Ciencias de la Naturaleza, Universidad Rey Juan Carlos, Tulipán s/n, 28933 Móstoles, Madrid, Spain

Fred Feudel
Institute of Physics, University of Potsdam, Am Neuen Palais 10, 14469 Potsdam, Germany

Miguel A. F. Sanjuán
Nonlinear Dynamics and Chaos Group, Departamento de Matemáticas y Física Aplicadas y Ciencias de la Naturaleza, Universidad Rey Juan Carlos, Tulipán s/n, 28933 Móstoles, Madrid, Spain

(Received 5 February 2003; accepted 16 June 2003; published 8 August 2003)

An analytical estimate of the width of the generated chaotic layer in a time-periodically driven stream function model for the motion of passive tracers is discussed. It is based essentially on the method of the separatrix map and the use of the Melnikov theory. Energy–time variables are used to derive lower bounds for the half width of the layer. In order to perform a comparison with numerical simulations, the results are transformed into space variables. The analytic results of the layer thickness in both parallel and perpendicular directions to the shear flow are compared with numerical computations and some systematic deviations are discussed. © *2003 American Institute of Physics.* [DOI: 10.1063/1.1598151]

The motion of passive tracers in a two-dimensional periodic incompressible fluid flow may possess a chaotic behavior, known as chaotic advection. This can be visualized in phase space as orbits forming a chaotic layer around a hyperbolic fixed point, where diffusion and transport properties are manifested. A stream function is derived as a "two-mode" truncation from a two-dimensional Navier–Stokes problem, in order to better understand the properties of the tracer dynamics under the influence of the chaotic saddle existing in phase space. As a matter of fact, the approximated stream function shows qualitatively the same dynamics as the full Navier–Stokes solution in the parameter region around the first bifurcations. By using an appropriate time-periodically driven stream function, we compute its Poincaré section and simulate the chaotic layer. This stream function can be considered as a time-dependent Hamiltonian, and consequently we can use analytical methods, such as Melnikov theory, in order to construct a separatrix map by which we can derive an analytical estimate of the stochastic layer width. The obtained analytical results are compared with the numerical results finding a rather good agreement with the half width parallel to the shear flow. We believe that our results might help one to better understand the validity of the separatrix map method for the analysis of the stochastic layer, especially when we trasform the original energy–time relations into phase–space relations.

I. INTRODUCTION

The dynamics of passive tracers in approximately two-dimensional fluid flows has been a subject of active research[1–3] since the publication of the seminal paper by Aref.[4] In particular, the formation of large scale spatial patterns, apparently as a result of inverse energy cascades,[5] has often been addressed within this context, both from an experimental and a theoretical viewpoint.[6] A widespread experimental setup used in the study of these coherent structures consists in an electrically conducting thin layer of fluid arranged along a set of magnets, so that the flow is driven by the Lorentz force. This generates a set of vortices in which it is possible to investigate the transitions produced when the applied current strength (and, consequently, the Reynolds number) is increased. First experiments in this direction were performed by Sommeria,[7] in which a square lattice of vortices was generated. In another series of experiments, Tabeling and co-workers studied these phenomena in a linear chain of forced vortices.[8–10]

Numerical simulations aimed at modeling these experiments were carried out in Refs. 11 and 12. More precisely, Ref. 11 accounts for the bifurcations of the lattice of forced vortices studied by Sommeria,[7] while Ref. 12 treats the case of a linear chain of forced vortices considered in the experiments by Tabeling and collaborators.[8–10] The dynamical models used in the numerical simulations of Refs. 11 and 12 are based on the two-dimensional Navier–Stokes equations, on which an external forcing is applied in order to drive a set of counter-rotating vortices. This resembles the initial experimental situation. By increasing the Reynolds number as the relevant control parameter, it was found that the first bifurcations were in good agreement with the experimental observations.

In the present paper, we will focus our attention on the behavior of the linear chain of vortices tackled in Ref. 12. The essential effect discussed in this reference is the genera-

tion of a shear flow produced by a merging of the counter-rotating vortices (called the primary steady state) to a chain of corotating vortices when the Reynolds number is increased. In this secondary state, the velocity field is still stationary. In a further Hopf bifurcation, the velocity field becomes time-dependent, oscillating periodically in time. In this work, we are interested in the tracer dynamics in this regime, where the velocity field varies regularly in time, but the motion of the tracers becomes already chaotic. Specifically, we study the width of the stochastic layer underlying such chaotic dynamics by means of an analytical approximation that allows a comparison with numerical simulations of the fluid flow directly in terms of the space coordinates $x-y$.

In order to examine more effectively the dynamics of passive tracers in the flow given by this time-dependent regime, a low dimensional stream function was derived in Ref. 13. The Lagrangian dynamics given by this stream function was then studied under the viewpoint of the existence of a chaotic saddle in phase space.[14–16] This low dimensional model is presented in Sec. II as the starting point of the present paper. Later, the stream function arising from this model is further simplified in Sec. III, in order to obtain the dynamical system that will be used in the analytical calculations performed in this work. In Sec. IV, the separatrix map technique and the Melnikov theory are applied to the Hamiltonian system given by the stream function derived in Sec. III, to obtain an analytical estimate for the width of the stochastic layer. In Sec. V, the results of Sec. IV are written in terms of spatial variables, with the aim of comparing with numerical computations. This allows a discussion on the validity of the method in simple terms. Finally, we provide some concluding remarks.

II. A FIVE-MODE STREAM FUNCTION

It is interesting to summarize here the main features of the low dimensional stream function model described in Ref. 13 in order to understand how the computations carried out in the present paper are in accordance with the experimental behavior shown in Refs. 8–10 and the numerical simulations of Ref. 12.

(1) Following Ref. 13, the first step in the derivation of this approximated model is to obtain a low dimensional stationary stream function that reproduces fairly well the streamlines of the flow in the secondary steady state (corotating vortices). This is done by selecting the first five modes in a pseudospectral expansion of the vorticity field of the flow in the parameter region around the first bifurcation. This procedure gives rise to an approximated stream function composed of the following five terms:

$$\begin{aligned}\Phi(x,y)=&\Phi_{(0,1)}\sin(y)+\Phi_{(0,3)}\sin(3y)\\&+\Phi_{(2,1)}\sin(2x)\sin(y)+\Phi_{(2,2)}\cos(2x)\sin(2y)\\&+\Phi_{(2,3)}\sin(2x)\sin(3y),\end{aligned}\tag{1}$$

where the indices of the stream function coefficients label the wave vector of the corresponding mode. In this way, the $\mathbf{k}=(2,1)$ mode represents the excitation of the driven counter-rotating vortices (this mode causes the primary steady state), the $\mathbf{k}=(0,1)$ and $\mathbf{k}=(0,3)$ modes give rise to the generated shear flow, and the $\mathbf{k}=(2,2)$ and $\mathbf{k}=(2,3)$ modes are responsible for the tilting of the eddies. Numerical computations show that this five-mode model is enough to capture more than 99% of the vorticity field of the fluid flow[13] of the secondary steady state (corotating vortices). Fixing the mode coefficients to values derived from the leading modes of the Navier–Stokes simulations,[17]

$$\begin{aligned}&\Phi_{(0,1)}=8.35,\quad \Phi_{(0,3)}=-0.35,\quad \Phi_{(2,1)}=-2.55,\\&\Phi_{(2,2)}=-0.81,\quad \Phi_{(2,3)}=0.25,\end{aligned}\tag{2}$$

it is found that the stream function of Eq. (1) reproduces correctly the streamlines of the Navier–Stokes flow in a stationary state below the Hopf bifurcation point.

(2) To establish an appropiate model of the time-dependent periodic solutions beyond the Hopf bifurcation, three features arising from the Navier–Stokes simulations are taken into account. First, the spatial structure of the velocity field is only slightly modulated by the time dependence. Second, the time scale of these variations is typically larger than the turnover time (a characteristic time scale which is set to be of the order of one). Third, the forced mode of the flow remains independent of time. It was found in Ref. 13 that a suitable choice that comprises these requirements can be achieved by periodically varying all the coefficients in Eq. (1), except the forced mode (2,1), as

$$\Phi_{(i,j)}(t)=\Phi_{(i,j)}[1+\delta\sin(\pi t)],\tag{3}$$

where δ is a constant that measures the strength of the modulation. Using this selection for the time-dependent perturbation, this five-mode model reproduces quite well the tracer dynamics of the fluid flow beyond the Hopf bifurcation. Similar models have been reported previously in the literature in somewhat different contexts (see, for example, Ref. 18).

In conclusion, the Lagrangian dynamics of the flow beyond the Hopf bifurcation is specified by the stream function model of Eq. (1), by the coefficients given in Eq. (2), and by the time variation of these coefficients according to Eq. (3). A picture showing the dynamics of passive tracers injected in this time-periodically varying stream function with $\delta=0.15$ is given in Fig. 2.

The most important qualitative difference between the tracer dynamics shown in Fig. 1, that is given by a stationary stream function and reproduces the flow below the Hopf bifurcation, and the tracer dynamics shown in Fig. 2, that is given by a time-periodically varying stream function and reproduces the flow beyond the Hopf bifurcation, is the existence of a stochastic layer in the second case, indicating that a chaotic dynamics appears. As mentioned before, the main motivation of the present work is to apply a known analytical method, based on the use of the Melnikov function and the separatrix map, to estimate the thickness of the stochastic layer in the case shown in Fig. 2 and, especially, to compare these estimations to numerical computations in order to establish some conclusions on the validity of this analytical method applied to this case.

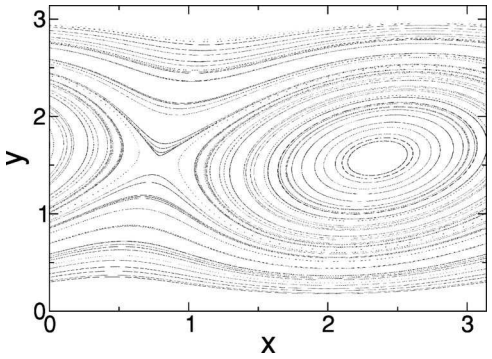

FIG. 1. Motions of passive tracers corresponding to the stationary state given by the five-mode stream function of Eq. (1) with the parameters chosen as in Eq. (2). As shown in Ref. 17, the streamlines depicted here qualitatively coincide with those obtained by means of direct numerical simulation of the Navier–Stokes equations.

With this objective in mind, a first difficulty appears: the dynamical system that describes the motion of passive tracers in the flow given by the time-periodically varying stream function consisting of five modes is too complicated to perform analytical computations with it. This is the main reason why we make a two-mode approximation to the five-mode stream function of Eq. (1), which is discussed in Sec. III.

III. A TWO-MODE STREAM FUNCTION

The analytical estimate of the stochastic layer width used in this work is based on the Melnikov approach. As is known, the computation of some exact solutions of the stationary part of the dynamical system is needed in order to use this method. The analytical computations of these solutions are not easy to do in the five-mode model defined by the stream function of Eq. (1), although certainly a numerical approach is possible. Since we are mainly interested in obtaining an analytical result, the first thing to do is to reduce this five-mode model further to a simpler model, while providing at the same time a good approximation for the stochastic layer of the flow.

We have reduced the five-mode stream function to an approximate two-mode stream function by neglecting three original modes in the following way.

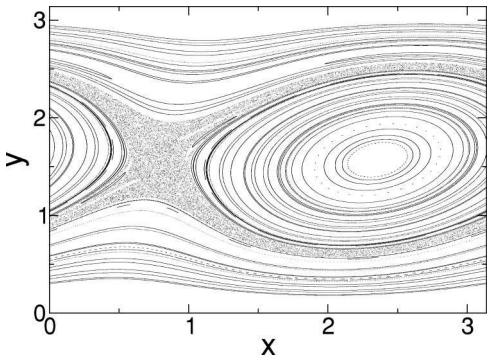

FIG. 2. Lagrangian dynamics of the time-periodically varying flow given by the stream function of the five-mode model in Eq. (1), with the coefficients given in Eq. (2), the time variation of these coefficients obeying Eq. (3), and $\delta=0.15$.

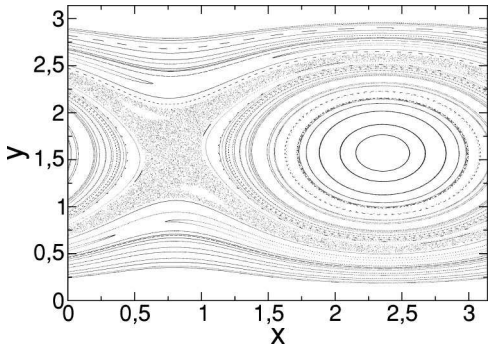

FIG. 3. Lagrangian dynamics of the time-periodically varying flow given by the two-mode stream function model with $\delta=0.15$. Comparing this figure with Fig. 2, corresponding to the five-mode stream function, a clear similarity is observed.

(1) As was said in Sec. I, the $\mathbf{k}=(2,2)$ and $\mathbf{k}=(2,3)$ modes in Eq. (1) cause the tilting of the eddies observed in the flow. These two modes can be neglected in a first approximation as this tilting affects only slightly the width of the stochastic layer.
(2) By contrast, the $\mathbf{k}=(2,1)$ mode, that represents the excitation of the driven counter-rotating vortices, is a basic ingredient in the flow, and so in the stochastic layer width.
(3) The $\mathbf{k}=(0,1)$ and $\mathbf{k}=(0,3)$ modes generate the shear flow. In this case, we neglect the $\mathbf{k}=(0,3)$ mode in a first approximation after comparing its relative importance to that of the $\mathbf{k}=(0,1)$ mode.

Consequently, the stream function of the two-mode model is reduced to

$$\Phi(x,y,t)=\Phi_{(0,1)}(t)\sin(y)+\Phi_{(2,1)}\sin(2x)\sin(y). \tag{4}$$

The flow generated by this stream function is periodic in x with a period of π. Following the arguments explained in the preceding section, only the $\Phi_{(0,1)}$ coefficient is varied periodically in this equation as

$$\Phi_{(0,1)}(t)=\Phi_{(0,1)}[1+\delta\sin(\pi t)], \tag{5}$$

where δ measures the strength of the modulation. The value of the parameters $\Phi_{(i,j)}$ are taken from Eq. (2), so $\Phi_{(0,1)}=8.35$ and $\Phi_{(2,1)}=-2.55$.

The motion of passive tracers in the two-mode stream function of Eqs. (4) and (5) is shown in Fig. 3 for $\delta=0.15$. It is interesting to compare this figure to Fig. 2, which corresponds to the five-mode stream function with the same δ. Numerical computations show that the difference between the stochastic layer width of the two-mode stream function and that of the five-mode stream function is smaller than 5% for the values of δ used in this work.

The velocity field or, equivalently, the equations of motion of the passive tracers can be expressed in the stream function formulation by

$$v_x=\dot{x}=\frac{\partial\Phi}{\partial y}, \quad v_y=\dot{y}=-\frac{\partial\Phi}{\partial x}, \tag{6}$$

which constitutes a Hamiltonian system. In order to simplify the notation, we consider all throughout the paper

$$a=\Phi_{(0,1)}=8.35, \quad b=-\Phi_{(2,1)}=2.55. \tag{7}$$

Then, the time-dependent Hamiltonian (or stream function) $H(x,y,t)=\Phi(x,y,t)$ can be written as the sum of a stationary term $\Phi_0(x,y)$, which is integrable, and a small time-dependent perturbation $\delta\,\Phi_1(x,y,t)$, which is not integrable,

$$H(x,y,t)=\Phi_0(x,y)+\delta\ \Phi_1(x,y,t), \tag{8}$$

$$\Phi_0(x,y)=\sin y(a-b\sin 2x), \tag{9}$$

$$\Phi_1(x,y,t)=a\sin y\sin \pi t. \tag{10}$$

We assume that δ is small in order to apply the Melnikov approach, which is a first-order perturbative method. Moreover, the phase space is considered to be the plane $[0,2\pi]\times[0,\pi]$, in order to include two of the hyperbolic fixed points of the unperturbed system. As we will see in Sec. IV, these points are key ingredients of the Melnikov method. In any case, the dynamical system given by Eqs. (8)–(10) is π-periodic in the x variable, so, for clarity, we depict only the $[0,\pi]\times[0,\pi]$ plane in the figures presented in this paper.

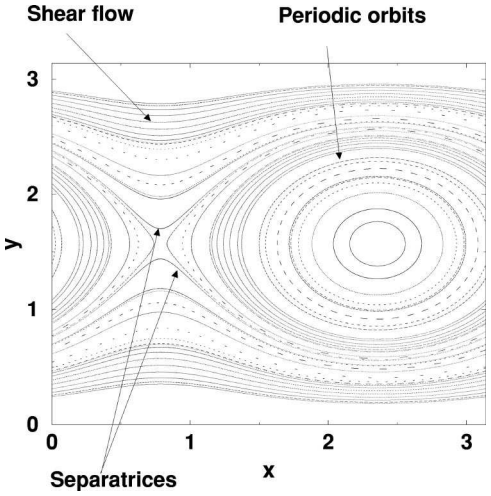

FIG. 4. Stroboscopic map for the two-mode unperturbed system ($a=8.35$, $b=2.55$) showing the different motions exhibited by the tracers at both sides of the separatrices. These lines are close to those signaled by the small arrows in the picture, but they cross each other in the hyperbolic fixed points $(\pi/4,\pi/2)$ and $(5\pi/4,\pi/2)$ (not shown).

IV. MELNIKOV METHOD, SEPARATRIX MAP, AND THE WIDTH OF THE STOCHASTIC LAYER

In this section we want to construct the separatrix map associated with the dynamics of the two-mode stream function model described in Sec. III. As is well known, a two-dimensional periodic vortical flow under a time periodic perturbation generally shows chaotic dynamics near the separatrix, in such a way that an appropriate description of the separatrix motion could be of importance for a better understanding of transport and diffusion properties within the stochastic layer.[19] The separatrix map was originally introduced by Zaslavsky and Filonenko[20] to investigate the one-dimensional motion of a charged particle in the field of a traveling wave under a perturbation. This map depends on the energy and time and approximately describes the regular and chaotic dynamics near a separatrix. In a subsequent work, the dynamics of the pendulum was analyzed by Chirikov[21] using the separatrix map. The importance of this map lies in the common features that its use can draw for a big classs of systems. For instance, some years ago, Chernikov *et al.*[22] used these ideas to obtain analytic expressions for the diffusion coefficients in the adiabatic regime of two-dimensional nonstationary flows. Another interesting application to a problem of chaotic advection can be found in Ref. 23. Likewise, Rom-Kedar[24,25] has used the separatrix map to classify two-dimensional time-periodic flows. In particular, we are interested in this map as a useful tool to compute an analytical estimate of the width of the stochastic layer, as is well described in Ref. 26 (see also Refs. 27 and 28 for complementary results).

The first step in order to construct the separatrix map is to analyze the unperturbed system, i.e., the case $\delta=0$. The trajectories in the phase space of this time independent flow (see Fig. 4) correspond to the level curves of the stream function $\Phi_0(x,y)$ given by Eq. (9). The dynamics of this integrable Hamiltonian system is essentially governed by two hyperbolic fixed points, $(x_1^*,y_1^*)=(\pi/4,\pi/2)$ and $(x_2^*,y_2^*)=(5\pi/4,\pi/2)$, that physically correspond to stagnation points in the flow, joined by two heteroclinic orbits called the separatrices of the unperturbed system. This name is due to the fact that the unperturbed heteroclinic orbits separate different kinds of motion in the phase space of the unperturbed system, as can be seen in Fig. 4. The central region bounded by both separatrices (that will be called the inner region) corresponds to periodic orbits around elliptic fixed points located at $(3\pi/4,\pi/2)$ and $(7\pi/4,\pi/2)$, and the region outside the separatrices (called the outer region) is full of shear-flow orbits.

The unperturbed system is integrable, and its associated energy is conserved, i.e., it is a conservative system (in this dynamical system, the unperturbed energy is taken to be the value of the stream function along its level curves). The value of the energy of any point belonging to the separatrices, including the hyperbolic fixed points, is given by

$$H_s=\Phi_0(x^*,y^*)=a-b, \tag{11}$$

which will be an important quantity in the discussion to follow. One key ingredient that we need in order to construct the separatrix map with the help of the Melnikov function is the explicit expression for the heteroclinic orbits. The equations of the heteroclinic orbits can be obtained by integrating the unperturbed two-mode system and have the following form:

$$x_s(t)=\frac{3\pi}{4}+\arcsin\left(\frac{\sinh(2\sqrt{b(a-b)}t)}{\sqrt{\cosh^2(2\sqrt{b(a-b)}t)-(b/a)}}\right), \tag{12}$$

$$y_s(t)=\frac{\pi}{2}\pm\arccos\left(\frac{\cosh^2(2\sqrt{b(a-b)}t)-(b/a)}{\cosh^2(2\sqrt{b(a-b)}t)+(b/a)}\right), \tag{13}$$

where the signs $\pm$ refer to each one of the heteroclinic orbits. Notice that these expressions are valid only if the condition $0<b<a$ holds, which is the case for the values given in Eq. (7). As is well known, the separatrices coincide in this

situation with the stable and unstable manifolds associated with the hyperbolic fixed points. However, when the time-dependent perturbation is introduced, the stable and unstable manifolds associated with one hyperbolic point break apart and might intersect transversely to each other,[29] generating a typical Smale horseshoe-type dynamics in the region near the separatrices. This phenomenon is typically related to a scenario of transient chaos. As said earlier, the description of the motions in this region, called the stochastic layer, is an important point for studying physical properties of the flow, such as transport and diffusion.

The Melnikov function is derived by using a first-order perturbation method, and is related to the distance (with sign) between the stable and the unstable manifolds associated with the hyperbolic fixed points of the system when the perturbation $\delta\Phi_1(x,y,t)$ is introduced. A detailed discussion on this issue is found in Ref. 30. An expression of the Melnikov function in terms of the heteroclinic orbits is given by

$$M(t_0)=\int_{-\infty}^{\infty} dt[\Phi_0(x_s(t),y_s(t)),\delta\Phi_1(x_s(t),y_s(t),t+t_0)], \tag{14}$$

where $x_s(t)$ and $y_s(t)$ are the explicit expressions for the separatrices of the unperturbed system, and $[\cdot,\cdot]$ denotes the Poisson bracket. The formation of the heteroclinic tangle which follows the transversal intersection takes place whenever $M(t_0)$ changes sign. After some algebraic manipulations, we can write the Melnikov function for both separatrices (indicated by $\pm$) as

$$M^{\pm}(t_0)=\pm\,\delta M_0(a,b)\cos\pi t_0, \tag{15}$$

where

$$M_0(a,b)=\frac{\pi^2 a}{\sqrt{a^2-b^2}}\frac{1}{\sinh\left(\dfrac{\pi^2}{4\sqrt{b(a-b)}}\right)} \times\sin\left(\frac{\pi}{4\sqrt{b(a-b)}}\operatorname{arg\,cosh}\frac{a+2b}{a}\right). \tag{16}$$

In this expression, it has been assumed that $0<b<a$, as pointed out earlier. Note also that, as can be easily seen in Eq. (15), the passage of $M^{\pm}(t_0)$ through zero is trivially guaranteed.

As we mentioned earlier, the regular and chaotic motion near the separatrices of nonlinear systems can be studied with the help of the separatrix map (for example, see, Ref. 31 for a rigorous approach to this problem). Using energy–time variables, it is possible to write the separatrix map as[26]

$$H_{n+1}=H_n+\Delta H_n(\tau_n), \tag{17}$$

$$\tau_{n+1}=\tau_n+\tfrac{1}{2}T(H_{n+1}), \tag{18}$$

in which the sequence of time instants (τ_j) correspond to half-periods $T/2$ of the unperturbed periodic orbits in the inner region near the separatrices. The derivation of the map involves the computation of the change ΔH_n in the energy of the orbit during the time step of the map. To accomplish this task, it should be taken into account that the time evolution of any dynamical variable is related to its Poisson bracket with the Hamiltonian. In this case, we have

$$\Delta H_n(\tau_n)=\int_{\tau_n-(1/4)\,T(H_n)}^{\tau_n+(1/4)\,T(H_n)} dt[\Phi_0,\delta\Phi_1]. \tag{19}$$

Since δ is a small parameter, and following the standard procedure, the map given by Eqs. (17) and (18) can be approximated near the separatrices by its value in the separatrix of the unperturbed system. This means that the limits of integration are extended to plus and minus infinity. As a consequence, the change of energy results to be equal to the previously computed Melnikov function,

$$\Delta H_n(\tau_n)=\int_{\tau_n-\infty}^{\tau_n+\infty} dt[\Phi_0(x_s,y_s),\delta\Phi_1(x_s,y_s,t+\tau_n)] =M^{\pm}(\tau_n). \tag{20}$$

For completeness, we should also compute the period of the unperturbed orbits in the inner region as a function of the energy of the unperturbed system H_s. We define the dimensionless variable

$$h_n=\frac{H_n}{H_s}-1=\frac{H_n}{a-b}-1,\quad |h_n|\ll 1. \tag{21}$$

In terms of this quantity, the period of an inner orbit very close to the separatrix in the unperturbed system, with energy $H=(a-b)(h+1)$ and $|h|\ll 1$, diverges as the function

$$T(h)=\frac{1}{\sqrt{b(a-b)}}\ln\left(\frac{16b}{a|h|}\right). \tag{22}$$

Thus it follows that the separatrix map for our system can be approximated as

$$h_{n+1}=h_n\pm\frac{\delta}{a-b}M_0\cos\pi\tau_n, \tag{23}$$

$$\tau_{n+1}=\tau_n+\frac{1}{2\sqrt{b(a-b)}}\ln\left(\frac{16b}{a|h|}\right). \tag{24}$$

This map provides some hints about the origin of chaotic dynamics in the stochastic layer.[32] Note that, in the region near an elliptic fixed point, the period of an orbit is weakly dependent on the energy, but in the separatrix region the period goes to infinity and, consequently, a small variation in the energy leads to a considerable change in the time variable of the map. By measuring the stretching of a small time interval with the quantity $K=\max|(d\tau_{n+1}/d\tau_n)-1|$, we claim that a local instability occurs when the heuristic condition $K\geqslant 1$ is satisfied.[26] This leads to an approximation for the width of the stochastic layer. A lower bound of the half-width of the stochastic layer, denoted by h_{sl}, is given, up to a constant of order 1, by

$$K(h_{\mathrm{sl}})=1. \tag{25}$$

In our case we obtain that the half-width of the stochastic layer is lower-bounded by

$$h_{\mathrm{sl}} = \delta \frac{\pi}{2(a-b)\sqrt{b(a-b)}} M_0, \tag{26}$$

where $M_0(a,b)$ is given by Eq. (16). Note that this measure has a linear dependence with the perturbation parameter δ, as shown in Eq. (26). This is a consequence of the method that we have used to derive this result, based on the Melnikov function, that is a first-order quantity in the perturbation parameter.

The use of the Melnikov method also poses a question about the range of δ values for which the approximation is valid. Taking into account that the energy of an unperturbed orbit very close to the separatrix is of order $(a-b)$, and that the perturbation is of order $\delta \cdot a$, the validity of the approach used here imposes the following condition:

$$\delta \cdot a \ll a - b, \tag{27}$$

from which it follows that $\delta \ll 0.7$, where a and b take the values of the original stream function given in Eq. (7).

Another interesting observation is related to the fact that this is an energy measure of the width, because the variable h_n in the separatrix map is related to the energy H_n through Eq. (21). Consequently, in order to compare this result with numerical computations, two ways can be followed. The first one is to perform numerical computations on the energy of the system itself. In this case, the approximate separatrix map, given by Eqs. (23) and (24), should not be used because it is an ingredient of the method that needs to be tested. The second way is to relate the analytical result of Eq. (26) to spatial quantities of the system in the phase space (x,y), where numerical computations are straightforward. The latter is the approach that we have used in this paper.

V. DISCUSSION AND COMPARISON WITH NUMERICAL COMPUTATIONS

In Sec. IV, we have used some analytical techniques to obtain an estimate of the quantity h_{sl} [Eq. (26)] that measures the half-width of the stochastic layer in the h axis of the plane (h,τ) given by the separatrix map. Due to the nature of the analysis performed there, this quantity does not have a direct visual interpretation and therefore it would be very interesting to relate this measure with the equivalent one in the $x-y$ space. Therefore, a view of how the stochastic layer looks in the (x,y) plane is crucial. This task must be achieved with the help of numerical simulations.

In order to understand the meaning of the analytical result given in Eq. (26), we have computed numerically the width of the stochastic layer in the $x-y$ space for several values of δ. We have done this by plotting a Poincaré section of a large number of trajectories starting from initial conditions lying on a grid within the domain $[0,\pi]\times[0,\pi]$. Note that we can restrict ourselves to this region due to the periodicity of the flow. Furthermore, note also that the referred domain contains one of the hyperbolic fixed points, $(\pi/4,\pi/2)$, in which the two separatrices intersect themselves in the unperturbed system. As we know, the stochastic layer appears when both separatrices cross each other an infinite number of times due to the perturbation. Then, this is the interesting region if one wants to measure the width of the stochastic layer. We have used a fourth-order Runge–Kutta integration scheme with a time step $\Delta t = 2\times 10^{-3}$ to simulate the dynamical evolution of Eqs. (6)–(10). Since the period of the forcing term is $T=2$, this choice of the time step allows one to obtain a stroboscopic map of the dynamics in a very simple way, with the advantage of a direct visualization of the stochastic layer (see Fig. 5). We have made two different measurements of the width of the stochastic layer. The distance, in the parallel direction to the shear flow, between the unperturbed hyperbolic fixed point and the right boundary of the layer is called l_x, which is a good approximation of the half width of the stochastic layer along the longitudinal direction to the shear flow. The distance, in the transverse direction to the shear flow, between the hyperbolic fixed point and the upper boundary of the layer is called l_y, which approximates the half width of the stochastic layer along the perpendicular direction to the shear flow (see Fig. 5). The numerical measurements for l_x and l_y when δ is varied from 0.025 to 0.250 are given in Table I.

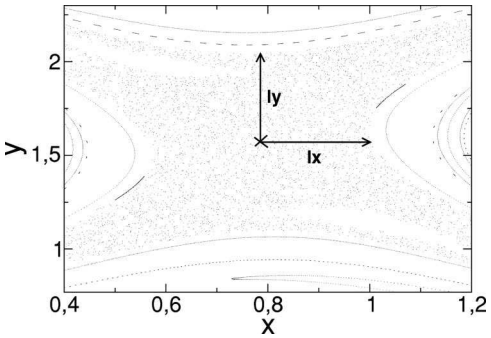

FIG. 5. A blow-up of the stochastic layer corresponding to a Poincaré section of the model described by Eqs. (6)–(10) for $a=8.35$, $b=2.55$, and $\delta=0.15$ is shown. The cross indicates the position of the hyperbolic fixed point $(\pi/4,\pi/2)$, whereas the arrows are depicted to illustrate the measures of the width of the stochastic layer carried out in the numerical simulations.

Going back to the problem of finding a relationship between the width of the stochastic layer in the $h-\tau$ space and the same quantity in the $x-y$ space will allow us to compare the numerics with the analytical estimate. In order to obtain

TABLE I. Numerical and analytical values of l_x and l_y, which represent the measures of the half width of the stochastic layer, for different values of the parameter δ ($a=8.35$ and $b=2.55$).

	Numerical		Analytical	
δ	l_x	l_y	l_x	l_y
0.025	0.1068	0.1462	0.0805	0.1067
0.050	0.1403	0.2003	0.1140	0.1509
0.075	0.1607	0.2558	0.1397	0.1850
0.100	0.1759	0.3893	0.1615	0.2137
0.125	0.2012	0.4185	0.1808	0.2390
0.150	0.2137	0.4473	0.1982	0.2619
0.175	0.2224	0.5001	0.2144	0.2831
0.200	0.2481	0.5508	0.2294	0.3027
0.225	0.3095	0.5947	0.2444	0.3223
0.250	0.3161	0.7231	0.2574	0.3393

such a relationship, we use the quantity h that appears in the separatrix map in relation to the energy of the system H,

$$h=\frac{H-(a-b)}{a-b}. \tag{28}$$

As a consequence, an interesting interpretation of h_{sl} is to consider it as the smallest difference between the energy of the unperturbed hyperbolic fixed point and the energy of a point that is at the boundary of the stochastic layer. Now, if we approximate the value of the energy by that of Φ_0, and use Eq. (9), we obtain that

$$h_{\mathrm{sl}}=\left|\frac{\sin y(a-b\sin 2x)-(a-b)}{a-b}\right|. \tag{29}$$

This is enough to relate h_{sl} to the numerical measurements. Remembering that l_x is the distance, in the parallel direction to the shear flow, between the unperturbed saddle and the right boundary of the stochastic layer, we can take $y=\pi/2$ along this direction, and $x=\pi/4+l_x$, so the previous equation gives

$$h_{\mathrm{sl}}=\left|\frac{2b}{a-b}\sin^2 l_x\right|. \tag{30}$$

In principle, this kind of argument can be used also with l_y. In this case, we can take $x=\pi/4$ and $y=\pi/2+l_y$, obtaining

$$h_{\mathrm{sl}}=|\cos l_y-1|, \tag{31}$$

but we will see later that only the first one, i.e., l_x, is correctly related to h_{sl}. In Table I we write the analytical values of l_x and l_y, i.e., those computed from Eqs. (30) and (31), and compare the results obtained using these expressions with the numerical computations.

By comparing the analytical and numerical results shown in Table I, some conclusions may be drawn. First, as a consequence of the way in which the analytical value of h_{sl} has been computed [Eq. (25)] and, especially, as a consequence of the way in which we have defined the quantities l_x and l_y through Eqs. (29)–(31), the analytical values of l_x and l_y are always a bit smaller than the numerical ones. Likewise, since our analytical method is a first-order perturbative one, we would expect that it will give a good approximation to l_x and l_y at least for small values of the perturbation strength δ. In Fig. 6, we can observe that for the values of δ considered here, the agreement between theory and numerics is rather good for l_x, that is, l_x is correctly estimated by the analytical method based on the separatrix map. At the same time, it becomes apparent that, even for very small values of the perturbation strength, the concordance between the lower bound given by Eq. (31) for l_y and the numerics is not as good as that of l_x (notice the different scales in the upper and lower panels of Fig. 6). Moreover, the analytical computation above $\delta\approx 0.08$ does not offer the qualitative behavior exhibited by the numerical values of l_y (note in Fig. 6 the apparent shift of these values near this value of δ).

As l_x is a measure of the stochastic layer width corresponding to the unperturbed inner region, and l_y is a measure in the unperturbed outer region, we conclude that the method of the separatrix map, applied to our system, gives a very good approximation to the half width of the stochastic layer, in phase variables, in the original inner region. On the other hand, the origin of the discrepancies found in the analytical measure in the outer region (corresponding to l_y) may be in the appearance of wide resonances (whose effects cannot be captured by the separatrix map) in this region as δ increases. These kinds of resonance have been analyzed for other Hamiltonian systems in Ref. 26 and also in Ref. 28, being able to cause discrepancies by a factor of 2 or more in the measurements of the stochastic layer.

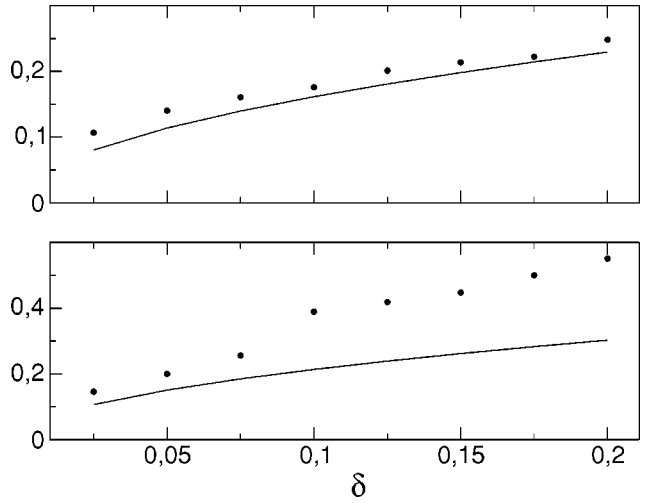

FIG. 6. Comparison of the computed half widths of the stochactic layer, parallel and perpendicular to the shear flow, for several values of δ, in the case $a=8.35$, $b=2.55$ corresponding to the two-mode model. Notice that the y scale in the upper panel is smaller than in the lower panel. Circles stand for numerical simulations values whereas the analytic approximation is given by the solid curve.

VI. CONCLUSIONS

In this paper we have obtained an analytical lower bound approximation to the widths of the stochastic layer, parallel and perpendicular to the shear flow, for a two-mode stream function model that reproduces the motion of passive tracers in a two-dimensional periodic flow. Using the Melnikov theory and the separatrix map in the standard way, we have obtained an approximation to the half width of the stochastic layer in the energy axis of the energy–time plane. Furthermore, we have related this measure with the equivalent one in the $x-y$ space for this particular model. This space seems to be a natural choice when chaotic transport of particles is considered, because it provides a direct visualization of the trajectories of the tracers. The values obtained by using this analytical approximation have been compared with numerical simulations of the model in order to test its validity.

On the one hand, we have found that this analytical method gives a rather good estimate of the first quantity, i.e., the half width parallel to the shear flow, l_x, for not very high values of the perturbation strength δ. On the other hand, it is also obtained that the analytical estimate does not give the correct values for the half width perpendicular to the shear flow, l_y. In particular, the values of l_y obtained from numerical simulations display a shift around $\delta\approx 0.08$ that is not seen in the analytical approximation. The origin of this dis-

crepancy may be the appearance of relatively wide resonances in the chaotic layer when δ increases.

These conclusions may help one to understand the meaning and the validity of the separatrix map technique as a method to study the stochastic layer in simple periodic systems. Especially, we would like to emphasize that an analytical estimate of the width of the stochastic layer in the spatial coordinates plane, which provides physical information about transport and diffusion properties, can be achieved.

ACKNOWLEDGMENTS

This work has been supported by an *Acción Integrada Hispano-Alemana* under Project No. HA2000-0018, by the Spanish Ministry of Science and Technology under Project No. BFM2000-0967, by the DAAD in the frame of the program *Acciones Integradas Hispano-Alemanas*, and by the Universidad Rey Juan Carlos under Project Nos. URJC-PGRAL-2001/02 and URJC-PIGE-02-04.

[1] J. M. Ottino, *The Theory of Mixing: Stretching, Chaos and Transport* (Cambridge University Press, Cambridge, 1989).
[2] *Chaos Applied to Fluid Mixing*, Chaos, Solitons and Fractals, Vol. 4, edited by H. Aref (Pergamon, Oxford, 1994), pp. 745–1116.
[3] H. Kellay and W. Goldburg, Rep. Prog. Phys. **65**, 845 (2002).
[4] H. Aref, J. Fluid Mech. **143**, 1 (1984).
[5] J. Paret and P. Tabeling, Phys. Rev. Lett. **79**, 4162 (1997).
[6] D. Rothstein, E. Henry, and J. P. Gollub, Nature (London) **401**, 770 (1999).
[7] J. Sommeria, J. Fluid Mech. **170**, 139 (1986).
[8] P. Tabeling, B. Perrin, and S. Fauve, Europhys. Lett. **3**, 459 (1987).
[9] P. Tabeling, O. Cardoso, and B. Perrin, J. Fluid Mech. **213**, 511 (1990).
[10] H. Willaime, O. Cardoso, and P. Tabeling, Phys. Rev. E **48**, 288 (1993).
[11] R. Braun, F. Feudel, and N. Seehafer, Phys. Rev. E **55**, 6979 (1997).
[12] R. Braun, F. Feudel, and P. Guzdar, Phys. Rev. E **58**, 1927 (1998).
[13] A. Witt, R. Braun, F. Feudel, C. Grebogi, and J. Kurths, Phys. Rev. E **59**, 1605 (1999).
[14] G. H. Hsu, E. Ott, and C. Grebogi, Phys. Lett. A **127**, 199 (1988).
[15] Á. Péntek, Z. Toroczkai, T. Tél, C. Grebogi, and J. A. Yorke, Phys. Rev. E **51**, 4076 (1995).
[16] M. A. F. Sanjuán, J. Kennedy, C. Grebogi, and J. A. Yorke, Phys. Rev. Lett. **78**, 1892 (1997).
[17] R. Braun, Ph.D. thesis, Universität Potsdam, 1997.
[18] T. H. Solomon and J. P. Gollub, Phys. Rev. A **38**, 6280 (1988).
[19] T. Ahn and S. Kim, Phys. Rev. E **49**, 2900 (1994).
[20] G. M. Zaslavsky and N. N. Filonenko, Sov. Phys. JETP **27**, 851 (1968).
[21] B. V. Chirikov, Phys. Rep. **52**, 263 (1979).
[22] A. A. Chernikov, A. I. Neishtadt, A. V. Rogal'sky, and V. Z. Yakhnin, Chaos **1**, 206 (1991).
[23] L. Kuznetsov and G. M. Zaslavsky, Phys. Rev. E **58**, 7330 (1998).
[24] V. Rom-Kedar, Physica D **43**, 229 (1990).
[25] V. Rom-Kedar, Nonlinearity **7**, 441 (1994).
[26] G. M. Zaslavsky, *Physics of Chaos in Hamiltonian Systems* (World Scientific, Singapore, 1998).
[27] D. Treschev, Physica D **116**, 21 (1998).
[28] A. C. J. Luo and R. P. S. Han, Chaos, Solitons Fractals **12**, 2493 (2001).
[29] R. Camassa and S. Wiggins, Phys. Rev. A **43**, 774 (1991).
[30] S. Wiggins, *Introduction to Applied Nonlinear Dynamical Systems and Chaos* (Springer, New York, 1990).
[31] D. Treschev, J. Nonlinear Sci. **12**, 27 (2002).
[32] M. Latka and B. J. West, Phys. Rev. E **52**, 3252 (1995).